nature metabolism

ARTICLES

https://doi.org/10.1038/s42255-019-0035-x

Ablation of adipocyte creatine transport impairs thermogenesis and causes diet-induced obesity

Lawrence Kazak[1,2*], Janane F. Rahbani[1,2], Bozena Samborska[1,2], Gina Z. Lu[3], Mark P. Jedrychowski[3], Mathieu Lajoie[1,2], Song Zhang[4], LeeAnn Ramsay[1,2], Florence Y. Dou[3], Danielle Tenen[5], Edward T. Chouchani[3], Petras Dzeja[4], Ian R. Watson[1,2], Linus Tsai[5], Evan D. Rosen[5] and Bruce M. Spiegelman[3*]

Depleting creatine levels in thermogenic adipocytes by inhibiting creatine biosynthesis reduces thermogenesis and causes obesity. However, whether creatine import from the circulation affects adipocyte thermogenesis is unknown. Here we show that deletion of the cell-surface creatine transporter (CrT) selectively in fat (AdCrTKO) substantially reduces adipocyte creatine and phosphocreatine levels, and reduces whole-body energy expenditure in mice. AdCrTKO mice are cold intolerant and become more obese than wild-type animals when fed a high-fat diet. Loss of adipocyte creatine transport blunts diet- and β3-adrenergic-induced thermogenesis, whereas creatine supplementation during high-fat feeding increases whole-body energy expenditure in response to β3-adrenergic agonism. In humans, *CRT* expression in purified subcutaneous adipocytes correlates with lower body mass index and increased insulin sensitivity. Our data indicate that adipocyte creatine abundance depends on creatine sequestration from the circulation. Given that it affects whole-body energy expenditure, enhancing creatine uptake into adipocytes may offer an opportunity to combat obesity and obesity-associated metabolic dysfunction.

The escalation in prevalence of obesity worldwide has led to a surge in type 2 diabetes, cardiovascular disease and many cancers[1,2]. Excess fat storage occurs when caloric intake persistently exceeds caloric expenditure[3]. The capacity for thermogenic adipose tissues (brown and beige) to dissipate chemical energy offers great potential to combat obesity. Some individuals who are predisposed to obesity exhibit decreased adipose thermogenic capacity[4], thus suggesting that this impairment is relevant in the context of human weight gain. Several pathways in adipose and non-adipose tissues have emerged in recent years and have been found to play critical roles in adaptive thermogenesis[5–11].

Creatine supports thermogenic respiration by stimulating mitochondrial ATP turnover in vitro[12,13]. Importantly, pharmacological reduction of endogenous creatine levels in adipocytes blunts adrenergic-stimulated thermogenesis and core body temperature in vivo, and reduces oxidative metabolism in beige fat and brown adipose tissue (BAT)[13–15]. Selective inactivation of creatine synthesis in fat (Adipo-Gatm knockout mice) causes a reduction in creatine levels in BAT, suppresses whole-body energy expenditure and results in obesity. Critically, creatine supplementation of Adipo-Gatm knockout animals prolongs the ability to sustain adrenergic thermogenesis, thus suggesting that creatine transport can be limiting under certain physiological conditions in vivo and that adipocyte creatine levels are at least partly regulated by sequestration from the circulation[16].

Results

Fat-selective deletion of the creatine transporter depletes adipocyte creatine abundance. Creatine can be taken up into cells by a creatine transporter, CrT (also known as *Slc6a8*)[17], and the rate of sequestration into BAT from the circulation is substantial, as it can match that of skeletal muscle[18]. To begin to examine the contribution of creatine transport to adipocyte creatine abundance, we purified the BAT stromal vascular fraction from mice containing a floxed allele of *CrT*[19], which we refer to as *CrT*$^{lox/y}$ mice. *CrT*$^{lox/y}$ primary brown adipocytes were differentiated in vitro and infected with adenovirus encoding Cre recombinase or green fluorescent protein (GFP). *CrT* transcript abundance was significantly reduced (~60%) 6 d after expression of CRE compared with expression of GFP (Fig. 1a). There was no defect in adipocyte differentiation of the cells on the basis of messenger-RNA expression levels of *AdipoQ*, *Fabp4* and *Pparg2* (Fig. 1a). Similarly, transcript levels of mitochondrial creatine kinases (*Ckmt1* and *Ckmt2*) and *Gatm* were not changed, but *Gamt* levels were marginally elevated. We also observed an increase in *Ucp1* mRNA abundance on *CrT* deletion (Fig. 1a). This potentially compensatory relationship between *Ucp1* and genes of creatine metabolism is consistently observed in various mouse models[13,16,20,21] and is suggestive of parallel thermogenic pathways.

Using liquid chromatography coupled to mass spectrometry (LC–MS), we detected a ~50% reduction in steady-state creatine and phosphocreatine (PCr) levels in CRE-infected *CrT*$^{lox/y}$ primary brown adipocytes compared with GFP-infected cells (Fig. 1b). In contrast, while CRE infection of *Gatm*$^{lox/lox}$ brown adipocytes reduced *Gatm* transcript abundance substantially, by 60% (Supplementary Fig. 1a), these adipocytes exhibited no change in creatine or PCr levels in vitro (Supplementary Fig. 1b). Thus, while the creatine pool in BAT is partly regulated by GATM-dependent creatine synthesis in vivo[16], creatine abundance is primarily regulated by cellular transport by CRT in cultured brown adipocytes

[1]Goodman Cancer Research Centre, McGill University, Montreal, Quebec, Canada. [2]Department of Biochemistry, McGill University, Montreal, Quebec, Canada. [3]Dana-Farber Cancer Institute, Department of Cell Biology, Harvard Medical School, Boston, MA, USA. [4]Department of Cardiovascular Medicine, Mayo Clinic, Rochester, MN, USA. [5]Division of Endocrinology, Beth Israel Deaconess Medical Center, Harvard Medical School, Boston, MA, USA. *e-mail: lawrence.kazak@mcgill.ca; bruce_spiegelman@dfci.harvard.edu

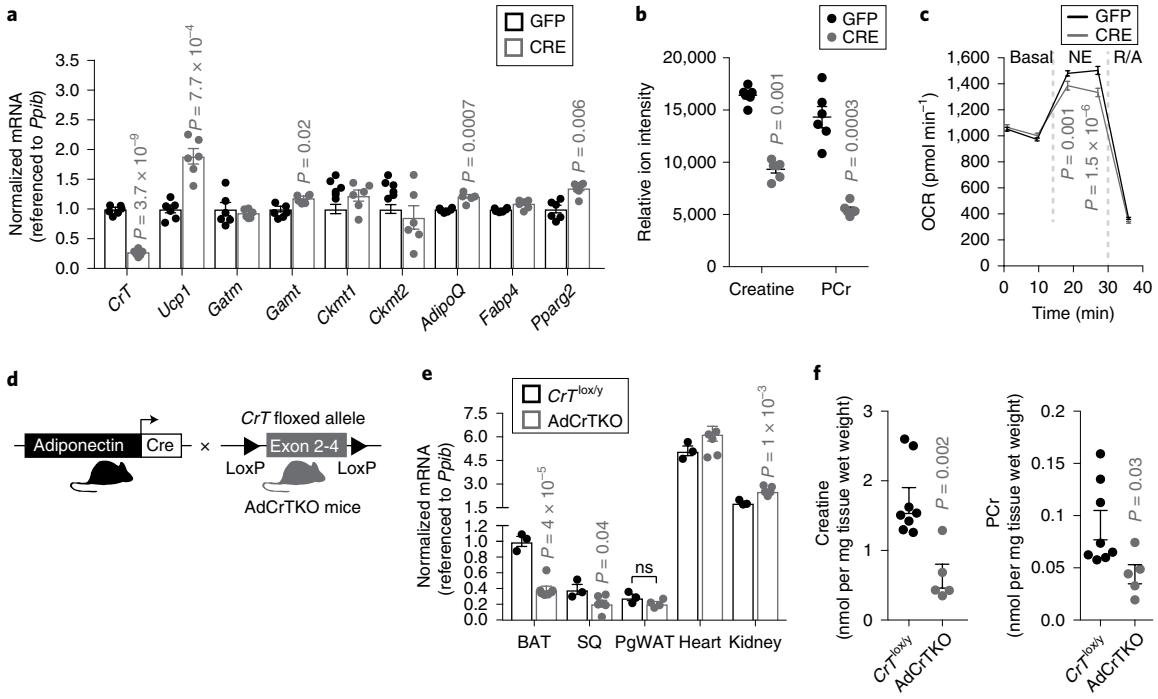

Fig. 1 | Inactivation of creatine transport depletes creatine abundance in adipocytes. a, RT-qPCR of primary brown adipocytes (genotype $CrT^{lox/y}$) after adenoviral-mediated infection with GFP or Cre recombinase (GFP, $n=6$; CRE, $n=6$). **b**, LC–MS analysis of creatine and phosphocreatine (PCr) levels after GFP or CRE adenoviral infection of $CrT^{lox/y}$ primary brown adipocytes (GFP, $n=6$; CRE, $n=6$). **c**, Oxygen consumption rate of GFP- or CRE-infected primary brown adipocytes (genotype $CrT^{lox/y}$) (GFP, $n=17$; CRE, $n=19$). Norepinephrine (NE) was added acutely at a final concentration of 100 nM. Rotenone and antimycin A (R/A) were used each at a final concentration of 3 μM to inhibit mitochondrial respiration. **d**, Cartoon of breeding strategy to generate adipose-specific *CrT* knockout mice (AdCrTKO). **e**, RT-qPCR of *CrT* mRNA from various tissues of $CrT^{lox/y}$ and AdCrTKO animals. Brown adipose tissue (BAT, $CrT^{lox/y}$, $n=3$; AdCrTKO, $n=7$), subcutaneous adipose tissue (SQ, $CrT^{lox/y}$, $n=3$; AdCrTKO, $n=6$), perigonadal white adipose tissue (PgWAT, $CrT^{lox/y}$, $n=3$; AdCrTKO, $n=4$), heart ($CrT^{lox/y}$, $n=3$; AdCrTKO, $n=7$) and kidney ($CrT^{lox/y}$, $n=3$; AdCrTKO, $n=7$). ns, not significant. **f**, NMR analysis of BAT creatine and PCr levels ($CrT^{lox/y}$, $n=8$; AdCrTKO, $n=5$). Data are presented as mean ± s.e.m. of biologically independent samples. Two-tailed Student's *t*-test (**a**–**c**,**e**,**f**).

in vitro. In agreement with a thermogenic role for creatine, CRE-infected $CrT^{lox/y}$ primary brown adipocytes exhibited decreased norepinephrine-dependent thermogenic respiration, as compared with GFP-infected cells (Fig. 1c).

We next explored the role of creatine transport-linked metabolism in vivo. We reduced the adipocyte creatine abundance through fat-selective inactivation of *CrT* by crossing Adiponectin-Cre transgenic animals[22] with $CrT^{lox/y}$ mice (Fig. 1d). We hereafter refer to this model as adipose-specific *CrT* knockout (AdCrTKO) mice. The selective deletion of *CrT* in adipocytes was evaluated by reverse transcription quantitative PCR (RT–qPCR) analysis of BAT, subcutaneous adipose tissue (SQ), perigonadal white adipose tissue (PgWAT), kidney and skeletal muscle. Significant depletion of *CrT* mRNA abundance was detected in bulk BAT and SQ of AdCrTKO animals relative to $CrT^{lox/y}$ controls (BAT: $CrT^{lox/y}$ 1.00 ± 0.06, AdCrTKO 0.39 ± 0.04; SQ: $CrT^{lox/y}$ 0.39 ± 0.06, AdCrTKO 0.21 ± 0.04) but not in PgWAT, kidney or skeletal muscle (Fig. 1e). Moreover, these data demonstrate that, of the adipose depots analysed, BAT displayed the highest *CrT* expression levels (approximately threefold higher than SQ and PgWAT).

We next determined whether *CrT* deletion perturbs creatine abundance in vivo. Indeed, creatine and PCr levels were significantly reduced in the BAT of AdCrTKO mice compared with $CrT^{lox/y}$ controls, as demonstrated by NMR (creatine: ~60% reduced; PCr: ~40% reduced) (Fig. 1f). Serum creatine levels were unaltered between AdCrTKO and $CrT^{lox/y}$ mice (Supplementary Fig. 1c), thus indicating that loss of adipocyte creatine does not alter systemic abundance of this metabolite. Our previous work with Adipo-Gatm knockout animals has shown that creatine is depleted by 30–40% in BAT[16]. Therefore, in terms of relative contributions of the different pathways for creatine accumulation, adipocyte creatine abundance is regulated by both intracellular synthesis and cellular transport in vivo.

AdCrTKO mice have impaired energy expenditure. Mice with adipocyte-specific loss of creatine synthesis are unable to maintain thermal homeostasis in response to acute cold (4 °C) exposure[16]. Thus, we explored body-temperature defence in AdCrTKO animals. On acute challenge to 4 °C, the body temperature of AdCrTKO mice dropped at a significantly faster rate than that of $CrT^{lox/y}$ control mice ($CrT^{lox/y}$ 35.1 °C ± 0.69 °C, AdCrTKO 33.6 °C ± 0.57 °C after 3 h) (Fig. 2a). These data indicate that loss of adipocyte creatine transport may impair thermogenic capacity in vivo. Thermogenic and non-thermogenic factors contribute to the maintenance of body temperature on exposure to decreased environmental temperature. Thus, we next studied whole-body energy expenditure by examining resting and adrenergic energy expenditure in animals relieved from thermal stress at thermoneutral (30 °C) housing[23]. Energy expenditure at rest during chow feeding was not different between AdCrTKO animals and littermate age-matched controls (Supplementary Fig. 2a), nor was there any difference between genotypes when accounting for any differences in body mass by analysis of covariance (ANCOVA) (Supplementary Fig. 2b). There was no difference in ambulatory movement between genotypes (Supplementary Fig. 2c). To examine the direct contribution of adipose tissue to whole-body metabolic rate, we used the relatively adi-

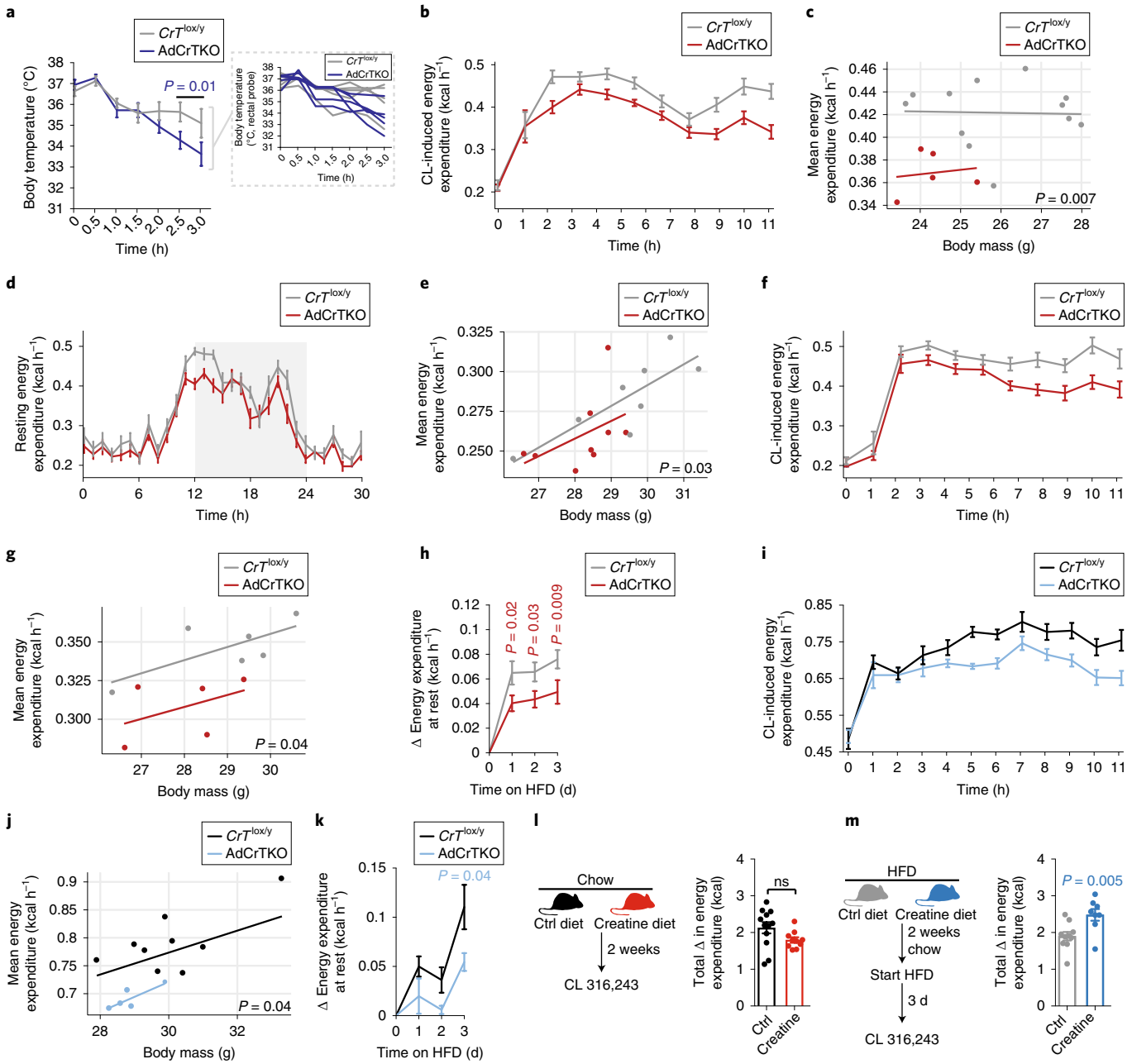

Fig. 2 | AdCrTKO mice have impaired energy expenditure. a, Body temperature of $CrT^{lox/y}$ and AdCrTKO mice ($n=5$ mice per genotype, individual mouse temperatures are shown in inset). **b**, Energy expenditure at 30 °C in response to CL 316,243 (CL) at 1 mg kg^{-1} ($CrT^{lox/y}$, $n=12$; AdCrTKO, $n=5$). **c**, Regression plot of data from **b** ($CrT^{lox/y}$, $n=12$; AdCrTKO, $n=5$). **d**, Resting energy expenditure in mice acutely (3 days) fed a high-fat diet at 30 °C ($CrT^{lox/y}$, $n=8$; AdCrTKO, $n=9$). **e**, Regression plot of data from **d** ($CrT^{lox/y}$, $n=8$; AdCrTKO, $n=9$). **f**, CL-dependent energy expenditure after acute high-fat feeding at 30 °C ($CrT^{lox/y}$, $n=6$; AdCrTKO, $n=5$). **g**, Regression plot of data from **f** ($CrT^{lox/y}$, $n=6$; AdCrTKO, $n=5$). **h**, Change in resting metabolic rate at 30 °C in response to high-fat feeding ($CrT^{lox/y}$, $n=7$; AdCrTKO, $n=9$). **i**, CL-dependent energy expenditure after acute high-fat feeding at 22 °C ($CrT^{lox/y}$, $n=9$; AdCrTKO, $n=5$). **j**, Regression plot of data from *i* ($CrT^{lox/y}$, $n=9$; AdCrTKO, $n=5$). **k**, Change in resting metabolic rate at 22 °C in response to high-fat feeding ($CrT^{lox/y}$, $n=11$; AdCrTKO, $n=4$). **l**, Experimental design for dietary chow creatine supplementation. Sustained energy expenditure (calculated as area under the curve) over 11 h after intraperitoneal (i.p.) administration of CL at 1 mg kg^{-1} (control chow diet, $n=12$; creatine-supplemented chow diet, $n=10$). **m**, Experimental design for dietary high-fat creatine supplementation. Sustained energy expenditure (calculated as area under the curve) over 11 h after i.p. administration of CL at 1 mg kg^{-1} (control high-fat diet, $n=10$; creatine-supplemented high-fat diet, $n=8$). Data are presented as mean ± s.e.m. of biologically independent samples. Multiple two-tailed Student's *t*-tests (**a**,**h**,**k**–**m**); ANCOVA (**c**,**e**,**g**,**j**).

pose-selective β3-adrenergic receptor agonist CL 316,243 (ref. [24]), which we refer to as CL. Because adrenergic responsiveness can be masked at subthermoneutral temperatures (when obligatory thermogenesis is not sufficient to maintain thermal homeostasis) we examined the change in energy expenditure of conscious free-moving mice housed at 30 °C after intraperitoneal administration of CL. Strikingly, the activation of CL-induced energy expenditure was significantly blunted (~10%) in AdCrTKO animals compared with $CrT^{fl/y}$ controls (Fig. 2b), thus confirming that loss of creatine transport impairs adrenergic thermogenesis in fat. Next, we applied

regression analysis to investigate the effect of inactivation of *CrT* on the relationship between CL-induced thermogenesis and body mass. The average energy expenditure per unit change in body mass was proportionately and significantly lower in AdCrTKO animals than their age-matched littermate controls (Fig. 2c). Thus, ablation of creatine transport into fat reduces whole-body metabolic rate in response to adrenergic stimulation.

Several genes involved in creatine metabolism are regulated at the mRNA level by acute caloric excess[16]. On the basis of this, we examined CRT protein abundance in purified brown adipocytes isolated from wild-type (C57BL6/N) mice after acute high-fat feeding for 3 d, by using liquid chromatography–tandem mass spectrometry (LC–MS/MS) high-resolution quantitative proteomics. Strikingly, CRT protein levels were significantly elevated (20%) after acute high-fat feeding (Supplementary Fig. 2d), a finding consistent with the idea that creatine transport may be important in triggering an increase in energy expenditure in response to caloric excess, known as diet-induced thermogenesis[16,25–27]. Thus, we began to explore the interaction of adipocyte creatine transport with diet-induced thermogenesis by examining resting metabolic rate[23] after acute exposure (3 d) to high-fat feeding. In contrast to chow feeding, acute high-fat feeding revealed a significant difference in resting metabolic rate between AdCrTKO animals and littermate age-matched controls (Fig. 2d), and this difference was maintained when accounting for any differences in body mass by ANCOVA (Fig. 2e). There was no difference in ambulatory movement between genotypes (Supplementary Fig. 2e). Moreover, adrenergic stimulation of adipocyte thermogenesis was reduced (~10%) in AdCrTKO animals compared with $CrT^{fl/y}$ controls (Fig. 2f); the average energy expenditure per unit body mass was proportionately and significantly lower in AdCrTKO animals than their age-matched littermate controls (Fig. 2g). Next, we monitored the resting metabolic rate of mice at 30 °C to determine the change in energy expenditure mediated by high-fat feeding itself. Strikingly, AdCrTKO mice had a blunted (~40%) ability to activate resting metabolic rate in response to high-fat feeding, as compared with $CrT^{lox/y}$ littermate controls (Fig. 2h and Supplementary Fig. 2f). Therefore, loss of adipocyte creatine transport impairs diet-induced thermogenesis.

We next explored the effect of *CrT* ablation on metabolic rate at standard temperature (22 °C) housing. The energy expenditure of chow-fed AdCrTKO mice was similar to that of $CrT^{lox/y}$ littermates at rest (Supplementary Fig. 2g), and when the variation in body mass of individual mice was accounted for by ANCOVA (Supplementary Fig. 2h). Moreover, the reduced energy expenditure on CL administration that we detected at 30 °C with chow-diet feeding was not present in chow-fed animals at 22 °C (Supplementary Fig. 2i,j). We hypothesized that the cold stress of 22 °C housing might mask adrenergic-mediated creatine-dependent thermogenesis, such that an additional (temperature-independent) thermogenic stimulus might be required to reveal the defect in whole-body energy expenditure of AdCrTKO animals. In agreement with this idea, AdCrTKO animals began to exhibit a trend towards reduced energy expenditure at rest, as compared with control mice, when fed a high-fat diet acutely (Supplementary Fig. 2k,l). However, this trend was not statistically significant. Strikingly, the activation of CL-induced energy expenditure was significantly blunted (~15%) in acute high-fat-diet-fed AdCrTKO animals compared with $CrT^{lox/y}$ controls (Fig. 2i). Regression analysis demonstrated that the average energy expenditure per unit change in body mass was proportionately lower in AdCrTKO animals than their age-matched littermate controls (Fig. 2j). Moreover, AdCrTKO mice exhibited reduced diet-induced thermogenesis, as compared with $CrT^{lox/y}$ animals at 22 °C (Fig. 2k and Supplementary Fig. 2m). Therefore, at 30 °C housing, decreased adrenergic thermogenesis is consistently observed in animals with depletion of adipocyte creatine stores, whether chow or high-fat fed. At 22 °C housing, the induction of diet-induced thermogenesis with acute high-fat feeding is required to reveal the impairment in adrenergic thermogenesis after depletion of BAT creatine.

Creatine supplementation increases energy expenditure during high-fat feeding. Since we hypothesized that creatine transport controls diet-induced thermogenesis, we explored the effect of dietary creatine supplementation on whole-body energy expenditure in wild-type mice. After two weeks of consuming creatine-supplemented diet (chow or chow followed by acute high fat), BAT creatine abundance was significantly higher than that in animals receiving no supplementation, as measured by LC–MS (Supplementary Fig. 2n). CL-induced activation of whole-body energy expenditure was not altered by creatine supplementation under chow-fed conditions (Fig. 2l). In contrast, it was significantly increased in creatine-supplemented animals after acute transition to high-fat diet, as compared with controls (Fig. 2m). Notably, creatine supplementation with acute high-fat feeding resulted in significantly higher BAT creatine levels than did creatine supplementation with chow diet (Supplementary Fig. 2n). Together, these data demonstrate that adipocyte creatine transport is critical for supporting diet-induced thermogenesis in vivo. This is caused by (1) an interaction between adipocyte creatine with certain components of high-fat diet, (2) increased sequestration of creatine into BAT on high-fat feeding or (3) a combination of the two.

AdCrTKO mice become more obese than control littermates on high-fat feeding. The decreased energy expenditure of AdCrTKO animals, particularly under high-fat feeding conditions, prompted us to explore their propensity for diet-induced obesity. AdCrTKO mice and age-matched $CrT^{lox/y}$ littermate controls were challenged with ad libitum feeding of high-fat diet over 8 weeks at two environmental temperatures (30 °C and 22 °C). At 30 °C housing, cumulative food intake was indistinguishable between AdCrTKO mice and $CrT^{lox/y}$ animals (Fig. 3a), whereas the body mass of AdCrTKO mice increased over controls (Fig. 3b). Metabolic efficiency is a hallmark of obesity[28], representing the fraction of assimilated energy that is stored somatically. AdCrTKO mice exhibited higher metabolic efficiency than $CrT^{lox/y}$ control mice ($CrT^{lox/y}$ 3.51 ± 0.55, AdCrTKO 5.26 ± 0.54) (Fig. 3c), strongly suggesting that fat-specific deletion of *CrT* may increase the propensity towards diet-induced obesity. In agreement with this hypothesis, AdCrTKO animals accreted a significantly greater quantity of fat mass than $CrT^{lox/y}$ animals (Fig. 3d), whereas lean mass was indistinguishable between genotypes (Supplementary Fig. 3a). Most striking was the triglyceride abundance in individual fat depots. In agreement with *CrT* deficiency causing adipocyte thermogenic impairment, the BAT triglyceride content from AdCrTKO animals was significantly greater (~fivefold) than BAT triglyceride content from $CrT^{lox/y}$ mice, and the SQ triglyceride content of AdCrTKO animals was nearly double that of $CrT^{lox/y}$ mice (Fig. 3e). The obese phenotype exhibited by AdCrTKO animals was not observed when these animals were fed a chow diet (Supplementary Fig. 3b,c). Similarly, there was no difference in lean mass between genotypes (Supplementary Fig. 3d).

At 22 °C housing, the cumulative food intake was identical between AdCrTKO mice and $CrT^{lox/y}$ animals (Fig. 3f), while the body mass of AdCrTKO mice trended higher than controls (Fig. 3g). AdCrTKO mice exhibited significantly higher metabolic efficiency than $CrT^{lox/y}$ control mice ($CrT^{lox/y}$ 3.2 ± 0.48, AdCrTKO 4.39 ± 0.30), a result further consistent with the hypothesis that deficiency in creatine transport into fat causes obesity (Fig. 3h). Indeed, the fat mass of AdCrTKO animals expanded more than the fat mass from $CrT^{lox/y}$ animals after high-fat feeding (Fig. 3i), whereas the lean mass was similar between genotypes (Supplementary Fig. 3e). BAT triglyceride levels from AdCrTKO animals were significantly greater (~threefold) than BAT triglyceride content from $CrT^{lox/y}$ mice, and

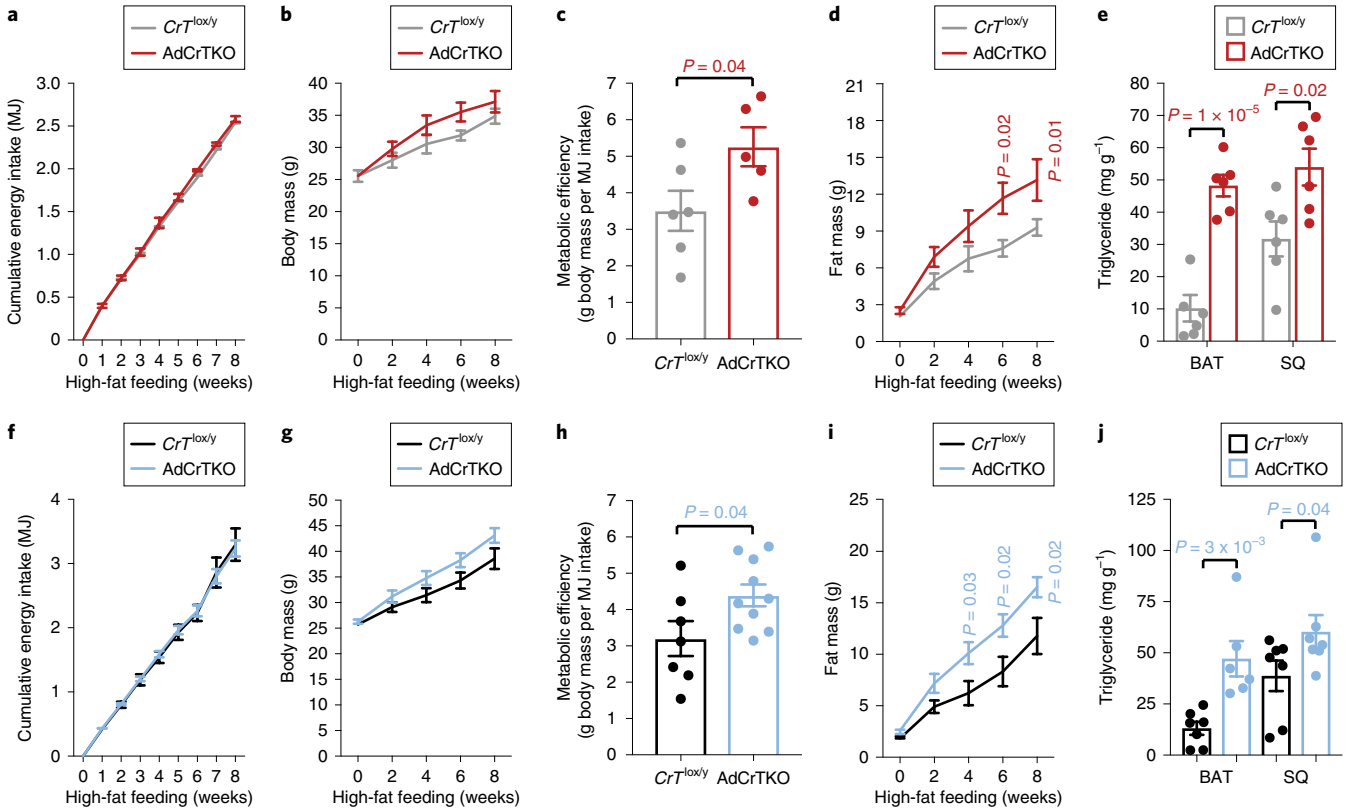

Fig. 3 | AdCrTKO mice become obese on a high-fat diet. a–d, Cumulative energy intake in megajoules (MJ) (**a**), body mass (**b**), metabolic efficiency (**c**) and fat mass (**d**) over 8 weeks of high-fat feeding at 30 °C ($CrT^{lox/y}$, $n=6$; AdCrTKO, $n=5$). **e**, Triglyceride abundance in BAT and SQ after 12 weeks of high-fat feeding at 30 °C (BAT and SQ: $CrT^{lox/y}$, $n=6$; AdCrTKO, $n=6$). **f–i**, Cumulative energy intake (MJ) (**f**), body mass (**g**), metabolic efficiency (**h**) and fat mass (**i**) over 8 weeks of high-fat feeding at 22 °C ($CrT^{lox/y}$, $n=7$; AdCrTKO, $n=10$). **j**, Triglyceride abundance in BAT and SQ after 8 weeks of high-fat feeding at 22 °C (BAT: $CrT^{lox/y}$, $n=7$; AdCrTKO, $n=6$; SQ: $CrT^{lox/y}$, $n=7$; AdCrTKO, $n=7$). Data are presented as mean ± s.e.m. of biologically independent samples. Two-tailed Student's *t*-tests (**c**,**h**); multiple two-tailed Student's *t*-tests (**a**,**b**,**d**–**g**,**i**,**j**).

SQ triglyceride content of AdCrTKO animals was nearly double that of $CrT^{lox/y}$ mice (Fig. 3j). Obesity did not occur in AdCrTKO mice fed chow diet (Supplementary Fig. 3f,g), nor was there a change in lean mass (Supplementary Fig. 3h). Thus, the consistent findings of obesity at the whole-body level and triglyceride accumulation in specific depots (BAT and SQ) at 30 °C and 22 °C, along with prior work[16], strongly indicate that adipocyte creatine depletion causes obesity, owing to increased metabolic efficiency and impaired diet-induced thermogenesis.

AdCrTKO mice exhibit increases in kininogen expression in BAT and SQ. Inactivation of creatine transport into adipose tissue did not alter *Ucp1* mRNA levels in BAT or SQ between AdCrTKO and $CrT^{lox/y}$ animals, regardless of housing temperature (Fig. 4a,b). Quantitative proteomics was next used to determine the global BAT expression profile of AdCrTKO animals compared with $CrT^{lox/y}$ littermate controls, housed at 30 °C or 22 °C. We were primarily interested in defining a common signature resulting from *CrT* inactivation, irrespective of housing temperature (Fig. 4c). In agreement with the mRNA levels, we did not detect any difference in BAT or SQ UCP1 protein expression between AdCrTKO and $CrT^{lox/y}$ animals, regardless of housing temperature (Fig. 4d,e), nor was there any significant difference in mitochondrial proteins (Supplementary Data 3), thus suggesting that the thermogenic impairment exhibited by AdCrTKO animals was not a result of reduced UCP1-dependent thermogenesis or general mitochondrial abundance. We identified 6,099 and 6,377 unique proteins from BAT of mice housed at 30 °C or 22 °C, respectively (Fig. 4c, Supplementary Data 1 and Supplementary Data 2). Intersection of these two datasets resulted in identification of 5,508 proteins (Fig. 4c and Supplementary Data 3). We next performed unbiased clustering of the samples by using proteins exhibiting the highest variance across all conditions and an empirical Bayes method to find proteins differentially expressed between AdCrTKO and $CrT^{lox/y}$ BAT consistently at 30 °C and 22 °C (Fig. 4f). This analysis yielded a set of 15 differentially expressed proteins at a false discovery rate (FDR) of 0.05 (Fig. 4g and Supplementary Fig. 3i). Gene ontology analysis on the differentially expressed proteins indicated an enrichment of proteins with known functions in the control of blood pressure (Fig. 4h). Specifically, kininogen 1 and 2 (KNG1 and KNG2) along with several kallikreins (involved in proteolytic processing of kininogens) were elevated in AdCrTKO compared with $CrT^{lox/y}$ BAT (Fig. 4g and Supplementary Fig. 3i). In agreement with elevated KNG1 expression in BAT, SQ from AdCrTKO animals also exhibited significantly elevated KNG1 protein expression at both 30 °C and 22 °C (Fig. 4i).

AdCrTKO mice incur adaptive increases in the cold-inducible high-molecular-weight isoform of *Kng1*. Adipose tissue plays an important role in maintaining vascular homeostasis[29], and BAT vasculature is critical for optimal thermogenic function. Obesity can impair BAT-mediated thermogenesis partly through capillary rarefaction, and obesity has been posited to be associated with impaired arterial distensibility[30,31]. In contrast, increasing BAT perfusion can increase glucose uptake into BAT, which may (indirectly) support thermogenic respiration[32,33]. However, *Kng1* mRNA has been identified in several reports to encode a BAT-enriched

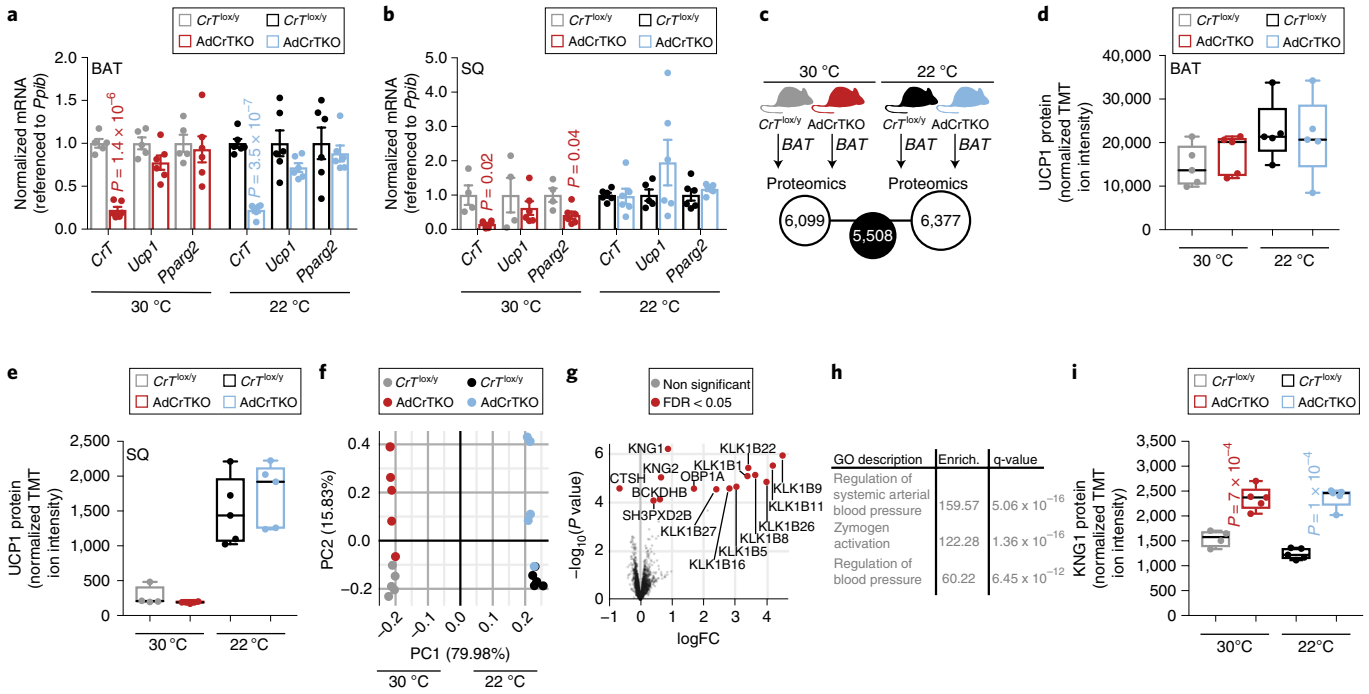

Fig. 4 | Increased kininogen expression from BAT and SQ of AdCrTKO mice. a, RT–qPCR from BAT of mice housed at 30 °C (*CrT*$^{lox/y}$, $n=5$; AdCrTKO, $n=6$), or 22 °C (*CrT*$^{lox/y}$, $n=6$; AdCrTKO, $n=6$). **b**, RT–qPCR from SQ of mice housed at 30 °C (*CrT*$^{lox/y}$, $n=4$; AdCrTKO, $n=6$), or 22 °C (*CrT*$^{lox/y}$, $n=6$; AdCrTKO, $n=6$). **c**, Cartoon of BAT proteomics experiment. **d**, Relative UCP1 protein abundance in BAT from mice housed at 30 °C (*CrT*$^{lox/y}$, $n=5$ (light grey); AdCrTKO, $n=5$ (red)) or 22 °C (*CrT*$^{lox/y}$, $n=5$ (black); AdCrTKO, $n=5$ (blue)). **e**, Relative UCP1 protein abundance in SQ from mice housed at 30 °C (*CrT*$^{lox/y}$, $n=4$ (light grey); AdCrTKO, $n=5$ (red)) or 22 °C (*CrT*$^{lox/y}$, $n=5$ (black); AdCrTKO, $n=5$ (blue)). **f**, Principal component analysis of proteomics results, using the 50 proteins with highest variance across all samples ($n=5$ mice per group). **g**, Volcano plot showing expression fold changes (FC) ($\log_2$) between AdCrTKO and *CrT*$^{lox/y}$ controls from both 30 °C and 22 °C housing, compared with their associated *P* values. Red dots represent proteins with significant changes at 0.05 FDR (*CrT*$^{lox/y}$, $n=10$; AdCrTKO, $n=10$). **h**, Gene ontology (GO) enrichment of differentially abundant proteins (*CrT*$^{lox/y}$, $n=10$; AdCrTKO, $n=10$). **i**, Relative KNG1 protein abundance in SQ from mice housed at 30 °C (*CrT*$^{lox/y}$, $n=4$ (light grey); AdCrTKO, $n=5$ (red)) or 22 °C (*CrT*$^{lox/y}$, $n=5$ (black); AdCrTKO, $n=5$ (blue)). Box plots were generated in Graphpad Prism by using default parameters. Boxes stretch from the twenty-fifth to the seventy-fifth percentile; black horizonal line within each box represents the median. Data are presented as mean ± s.e.m. of biologically independent samples. Two-tailed Student's *t*-tests (**a**–**d**,**i**); moderated *t*-tests using the limma (v3.32.10) package in R[51,52] as justified in ref. [53] (**g**); hypergeometric test implemented in the GOrilla tool (**h**); *q* values and FDR obtained by using the Benjamini–Hochberg approach (**g**,**h**).

secreted protein, and to be elevated in SQ fat on cold exposure[34,35], thereby suggesting that KNG1 may have a thermogenic function. Thus, kininogen upregulation in AdCrTKO BAT and SQ suggested that this was an adaptive response that counters the impaired thermogenesis caused by creatine depletion. Alternative splicing leads to two *Kng1* isoforms, yielding a high-molecular-weight kininogen and a low-molecular-weight kininogen. Using RT–qPCR, we compared the mRNA abundance of *Kng1* and *Kng2* between AdCrTKO and *CrT*$^{lox/y}$ BAT. We detected a significant increase in *Kng1* mRNA abundance in AdCrTKO compared with *CrT*$^{lox/y}$ BAT, when using primers detecting all *Kng1* isoforms or primers specific to the high-molecular-weight isoform (Fig. 5a). In contrast, the low-molecular-weight isoform of *Kng1*, as well as *Kng2*, were not differentially expressed at the mRNA level (Fig. 5a). These data suggest that in AdCrTKO BAT, KNG1 and KNG2 protein upregulation (Fig. 4g) is at least partly regulated at the transcriptional and post-transcriptional level, respectively, and that the high-molecular-weight KNG1 isoform is the primary KNG1 isoform elevated in response to creatine depletion in adipose tissue.

Next, we examined the expression of *Kng1* and *Kng2* mRNA between different fat depots, as well as their regulation following acute and chronic exposure to cold (4 °C), compared with 30 °C housing. *Kng1* and *Kng2* expression was highly enriched in BAT, compared with SQ and PgWAT (Fig. 5b). Furthermore, abundance of the high-molecular-weight isoform of *Kng1* was significantly increased in BAT, SQ and PgWAT after 4 °C exposure (Fig. 5c). *Kng2* levels were significantly elevated in SQ and PgWAT (but not BAT) on exposure to environmental cold (Fig. 5c). Together, our findings and the findings of others[34,35] suggest a potential role for kininogens (particularly KNG1) in adaptive thermogenesis. If true, elevated KNG1 and KNG2 abundance at the protein level in AdCrTKO BAT is consistent with an adaptive response resulting from impaired creatine-dependent thermogenesis.

***CRT* levels in human adipocytes correlate with lower body mass index and increased insulin sensitivity.** Creatine metabolism is selective for BAT compared with white fat in humans[8,36]. A recent analysis of ~2,850 [^{18}F]fluorodeoxyglucose positron-emission tomography/computed tomography scans from 1,644 human subjects has demonstrated that BAT creatine energetics may be a significant predictor of total activated human BAT[37]. Moreover, in a recent study of human BAT-mediated postprandial thermogenesis, 52 genes have been found to be significantly correlated with *UCP1* expression, two which are the mitochondrial creatine kinases (*CKMT1A* and *CKMT2*)[38]. We investigated the expression of genes that regulate the abundance of creatine in purified human subcutaneous adipocytes of 43 patients with a wide body mass index (BMI) range, who were undergoing elective plastic surgery. A diagnosis of diabetes was a criterion for exclusion, as the focus here was on proximal changes associated with obesity and insulin resistance, rather than downstream changes resulting from hyperglycaemia (and drug treatments). We compared the mRNA expression of genes

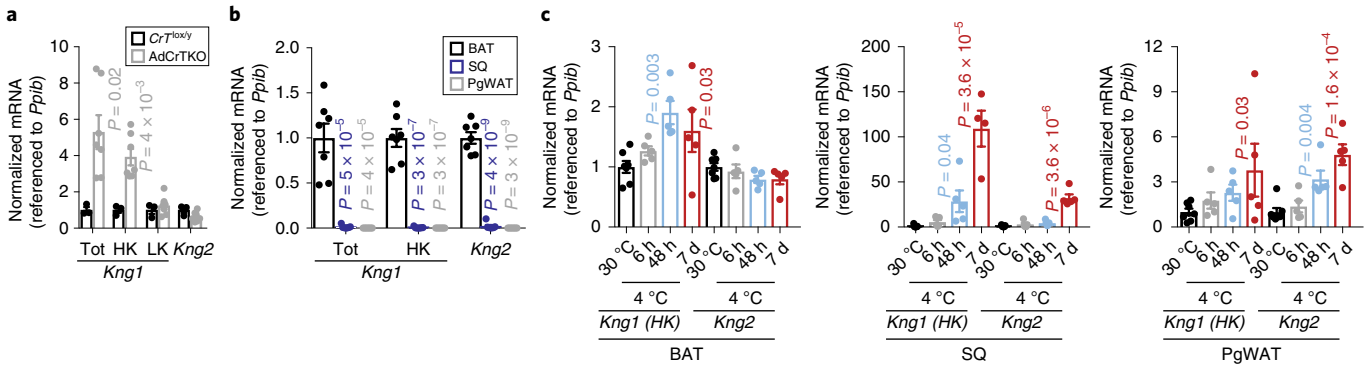

Fig. 5 | AdCrTKO mice incur adaptive increases in the cold-inducible high-molecular-weight isoform of *Kng1*. **a**, RT–qPCR of kininogen isoforms in BAT ($CrT^{lox/y}$, $n=3$; AdCrTKO, $n=7$). **b**, RT–qPCR of kininogen isoforms from mice housed at 30 °C ($n=7$). **c**, RT–qPCR of kininogen isoforms from mice housed at 30 °C ($n=7$) or exposed to 4 °C for 6 h ($n=5$), 48 h ($n=5$), and 7 d ($n=5$). Data are presented as mean ± s.e.m. of biologically independent samples. Two-tailed Student's *t*-tests (**a**); one-way analysis of variance (ANOVA) (**b**,**c**). HK, high-molecular-weight kininogen; LK, low-molecular-weight kininogen.

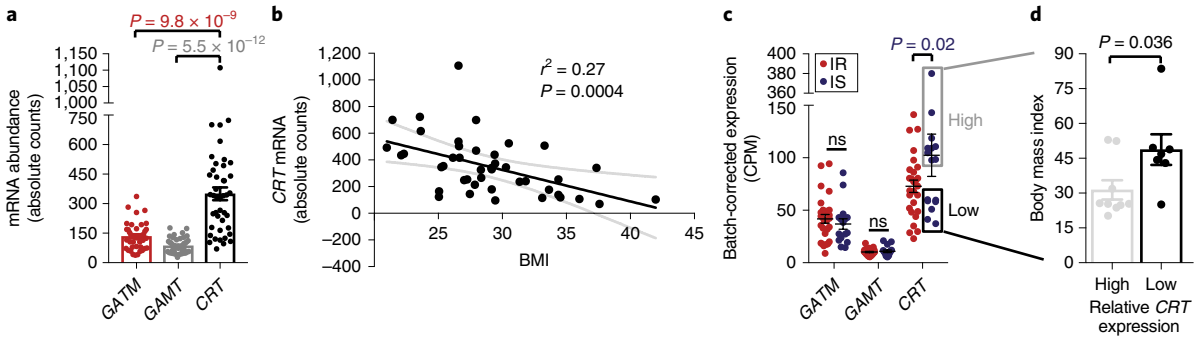

Fig. 6 | *CRT* expression in human adipocytes is negatively correlated with obesity and insulin resistance. **a**, mRNA abundance of *GATM*, *GAMT* and *CRT* by RNA sequencing ($n=43$). **b**, Pearson correlation of *CRT* mRNA expression with BMI ($n=43$). Black line, linear regression; grey curved lines, 95% confidence intervals. **c**, mRNA abundance of *GATM*, *GAMT* and *CRT* in patients stratified as insulin resistant (IR) and insulin sensitive (IS) (IS, $n=16$; IR, $n=27$). **d**, BMI of IS patients with relatively high ($n=9$) or low ($n=7$) *CRT* mRNA abundance. Data are presented as mean ± s.e.m. of biologically independent samples. One-way ANOVA (**a**); Pearson correlation (**b**); multiple two-tailed Student's *t*-tests (**c**); two-tailed Student's *t*-tests (**d**).

that regulate creatine abundance (*CRT*, *GATM* and *GAMT*) by RNA sequencing. *CRT* was the most abundant, followed by *GATM* and then *GAMT* (Fig. 6a). Strikingly, *CRT* abundance was inversely and significantly correlated with the BMI of patients (Fig. 6b), thus suggesting a possible causal relationship between decreased creatine transport and human obesity. Furthermore, when patients were stratified into insulin-sensitive and insulin-resistant groups, *CRT* expression was significantly lower in insulin-resistant patients than insulin-sensitive patients, whereas *GATM* and *GAMT* expression was not different between these groups (Fig. 6c). Finally, the insulin-sensitive group could be substratified into those with relatively low or high *CRT* expression. The subgroup with low *CRT* expression had a significantly greater BMI than the subgroup with high *CRT* expression (Fig. 6c,d). Thus, the strong inverse correlation of *CRT* transcript levels with BMI and insulin resistance suggests that creatine transport-mediated energetics plays an important role in human adipocyte metabolism. Importantly, the insulin-sensitive subgroup data (Fig. 6d) indicate that *CRT* expression can be uncoupled from insulin resistance, but not BMI, thus suggesting that creatine energetics is primarily associated with obesity and that insulin resistance may arise consequently, secondary to obesity, in the population with low *CRT* expression.

Discussion

Several properties of creatine transport suggest that it functions as a mediator for diet-induced thermogenesis: (1) it is required to support full thermogenic activation on pharmacological adrenergic stimulation, (2) its loss substantially reduces activation of whole-body energy expenditure in response to caloric excess, (3) selective modulation of energy expenditure by creatine occurs primarily during high-fat feeding, and (4) loss of creatine transport increases metabolic efficiency without effecting food intake, thus leading to obesity. It is important to note that creatine-dependent thermogenesis does not require *Ucp1* inactivation to reveal its physiological relevance, and UCP1 protein levels are even modestly elevated in BAT of AdCrTKO animals compared with $CrT^{lox/y}$ littermates.

While we detected a statistically significant decrease (80%) in BAT *CrT* mRNA levels at both 30 °C and 22 °C, *CrT* abundance was only significantly reduced (85%) in SQ from animals housed at 30 °C (Fig. 4b). Interestingly, conditions in which CL-dependent energy expenditure is lower in AdCrTKO mice compared with controls (Fig. 2b,f,i and Supplementary Fig. 2i) correspond well with conditions in which *CrT* abundance is significantly reduced in both BAT and SQ (Fig. 4a,b). These data support the idea that BAT and SQ may both contribute to creatine-dependent thermogenesis.

It is still debated what rodent housing temperature most precisely mimics human thermal conditions[39,40]. The results presented herein were derived from experiments conducted at 30 °C and 22 °C, and so the drive for heat production to combat heat loss was either eliminated or mildly present, respectively. Importantly, irrespective of housing temperature, adipocyte creatine transport is critical for

mitigating fat mass gain, thus indicating that it may have important clinical relevance to human obesity.

Our and others' prior work, using in vitro and chemical approaches, has suggested a critical role for adipose tissue creatine metabolism in enhancing energy expenditure through stimulation of ATP turnover[8,12–16,36,41]. While the phenotype of the currently available tissue-specific genetically engineered mouse models (Adipo-Gatm knockout and AdCrTKO) substantiate the initial mechanistic interpretations in isolated mitochondria, it is currently unknown whether the thermogenic role for creatine in vivo is more complex than the proposed mechanism of mitochondrial ATP turnover. This is the focus of our current research efforts. Nevertheless, evidence in support of creatine playing a key role in adipocyte thermogenesis has accumulated in recent years from work independent from ours. Global *CrT* knockout mice, which exhibit similar levels of creatine depletion to those of Adipo-Gatm knockout and AdCrTKO animals, have greater body fat stores than controls, despite a decrease in food intake[42]. Creatine kinase U-type (*Ckmt1*) and brain-type creatine kinase (*Ckb*) double-knockout animals are cold sensitive and have an impaired capacity to activate thermogenic respiration in response to norepinephrine administration[43], thus providing additional supporting evidence for a role of creatine metabolism in thermoregulation in vivo. Future work in this area will require the generation of new animal models with fat-selective creatine kinase deletion. These models will undoubtedly be useful to further delineate the molecular mechanism of creatine-dependent thermogenesis and its role in obesity and metabolic disease. The current findings, in conjunction with previous work from our group and others, place adipocyte creatine energetics as a central regulator of whole-body energy expenditure and obesity.

Methods

Animals. Mice were housed at 22 °C under a 12-h light/dark cycle and given free access to food and water until 8 weeks of age. $CrT^{lox/y}$ animals were obtained from the Jackson Laboratory (B6(SJL)-*Slc6a8*$^{tm1.1Clar}$/J, stock. 020642). Adiponectin-Cre mice (B6;FVB-Tg(*Adipoq-cre*)1Evdr/J, stock 028020), maintained on a C57BL/6J background, were bred to $CrT^{lox/y}$ animals to generate experimental groups. All experiments used age-matched male littermates and were conducted at either 30 °C or 22 °C. Animals were housed in groups of three unless otherwise stated. Animal experiments were performed according to procedures approved by the Animal Resource Centre at McGill University and complied with guidelines set by the Canadian Council of Animal Care. Experiments were performed according to procedures approved by the Institutional Animal Care and Use Committee of the Beth Israel Deaconess Medical Center.

High-fat feeding. AdCrTKO mice and age-matched littermate controls ($CrT^{lox/y}$) were genotyped at 2 weeks of age. At 3 weeks of age, mice were weaned by genotype into groups of three per cage, where they were housed at 22 °C and fed a chow diet. Mice of different genotypes were housed in cages side by side to limit variability in exposure to differential temperatures within the housing facility. At 8 weeks of age, mice (housed three per cage) were either transferred to incubators set at 30 °C or maintained in the housing room at 22 °C. The high-fat diet (initiated at 8 weeks of age) was a rodent diet (OpenSource Diets, D12492) with 60% kcal fat, 20% kcal carbohydrate and 20% kcal protein. C57BL/6NJ mice (Jackson Laboratory; stock 005304) were used as wild-type mice for examining CRT protein levels after acute high-fat feeding.

Calorimetric measurements. Indirect calorimetry studies were conducted at the Brigham and Women's Hospital Metabolic Core facility. Animals were housed individually in metabolic chambers maintained at 30 °C or 22 °C under a 12-h light/dark cycle and given free access to food and water. The mice were acclimated to metabolic cages for 24 h before measurements. Whole-body metabolic rate was measured by using an Oxymax open-circuit indirect calorimeter, Comprehensive Lab Animal Monitoring System (Columbus Instruments), available to the Brigham and Women's Hospital Metabolic Phenotyping Core.

Diet-induced thermogenesis. Animals were housed individually in metabolic chambers maintained at 30 °C or 22 °C under a 12-h light/dark cycle and given free access to food and water. The resting metabolic rate at each ambient temperature (30 °C or 22 °C) was calculated from the mean of three lowest energy expenditure (kcal) readings. Change in energy expenditure (kcal) in response to high-fat feeding was plotted as the absolute increase in resting metabolic rate from the last day of chow feeding.

Metabolic efficiency. Metabolic efficiency was measured as body mass accumulation as a function of cumulative energy intake.

Body composition. Body composition was examined with Echo MRI (Echo Medical Systems) by using a 3-in-1 Echo MRI Composition Analyzer.

Adrenergic activation of metabolic rate. Animals were housed individually in metabolic chambers maintained at 30 °C or 22 °C under a 12-h light/dark cycle and given free access to food and water. Mice were injected with CL 316,243 (dissolved in saline) intraperitoneally at 1 mg kg^{-1} at 6:00 hours. Mice were subsequently placed back in their metabolic cages, and oxygen consumption was monitored.

Metabolite analyses of primary brown adipocytes by mass spectrometry. Creatine and phosphocreatine were profiled with General Metabolics, LLC, and executed at General Metabolics laboratories according to previously published methodology[44]. Briefly, 2×10^6 adipocytes were washed three times with fresh pre-warmed (37 °C) 75 mM ammonium carbonate, pH 7.4. Metabolites were extracted with 700 µl of pre-heated (75 °C) extraction solvent (70% (v/v) ethanol (absolute) in HPLC-grade water). Extraction solvent was kept on cells for 3 min. Samples were rapidly transferred to a dry ice/ethanol bath. Samples were centrifuged 16,000*g* for 10 min at 4 °C. An equal volume of extract supernatant was recovered and stored at −80 °C until metabolite analysis. Analysis was performed on a platform consisting of an Agilent Series 1100 LC pump coupled to a Gerstel MPS2 autosampler and an Agilent 6520 Series Quadrupole time-of-flight mass spectrometer equipped with an electrospray source operated in negative and positive mode. The flow rate was 150 µl min^{-1} of mobile phase consisting of isopropanol/water (60:40 (v/v)) buffered with 5 mM ammonium carbonate at pH 9 for negative mode and methanol/water (60:40 (v/v)) with 0.1% formic acid at pH 3 for positive mode. For online mass axis correction, 2-propanol (in the mobile phase), taurocholic acid and hexakis(1H,1H,3H-tetrafluoropropoxy)phosphazine (HP-0921, Agilent Technologies) for negative mode and creatinine, reserpine and HP-0921 for positive mode were added to the mobile phase. Mass spectra were recorded in profile mode from m/z 50 to 1,000 with a frequency of 1.4 spectra per second for 0.48 min, by using the highest resolving power (4 GHz HiRes). The source temperature was set to 325 °C with 51 min^{-1} drying gas and a nebulizer pressure of 30 psig. Fragmentor, skimmer and octopole voltages were set to 175, 65 and 750 V, respectively.

Metabolite analyses of BAT by mass spectrometry. Creatine was profiled at the Rosalind and Morris Goodman Cancer Research Centre Metabolomics Core Facility. Briefly, BAT (10 mg) was combined with 1.14 ml of methanol/HPLC-grade water (50:50 (v/v)), 0.66 ml of ice-cold acetonitrile (ACN) (at −20 °C or colder) and four ceramic beads (2.8-mm diameter). The mixture was homogenized in a bead beater (Qiagen TissueLyser) for 2 min at 30 Hz. Next, samples were transferred into a 5-ml tube containing 1.8 ml of ice-cold dichloromethane and 0.9 ml of ice-cold HPLC-grade water. The samples were vortexed for 1 min, incubated on ice for 10 min and centrifuged at 4,000 r.p.m. for 10 min at 1 °C. Water-soluble metabolites in the upper polar phase were collected and dried by using a chilled ASpeedVac set at 4 °C. Samples were resuspended in 50 µl of HPLC-grade water before LC–MS analysis. For targeted metabolite analysis and semi-quantitative concentration determination of creatine, samples were injected onto an Agilent 6430 Triple Quadrupole (QQQ)–LC–MS/MS. Chromatography was achieved by using a 1290 Infinity ultra-performance LC system (Agilent Technologies) consisting of vacuum degasser, autosampler and a binary pump. The mass spectrometer was equipped with an electrospray ionization source, and samples were analysed in positive mode. Multiple reaction monitoring was optimized on authentic metabolite standards. The quantifying and qualifying ion transitions for creatine were 132.1→90.1 and 132.1→44.2, respectively. The source-gas temperature and flow were set at 350 °C and 10 l min^{-1}, respectively, the nebulizer pressure was set at 40 psi, and capillary voltage was set at 3,500 V. Chromatographic separation of creatine was achieved by using an Intrada Amino Acid column, 3 µm, 3.0×150 mm^2 (Imtakt Corp.). The chromatographic gradient started at 100% mobile phase B (0.3% formic acid in ACN) with a 3-min gradient to 27% mobile phase A (100 mM ammonium formate in 20% ACN/80% water) followed with a 19.5-min gradient to 100% A at a flow rate of 0.6 ml min^{-1}. This was followed by a 5.5-min hold time at 100% mobile phase A and a subsequent re-equilibration time (7 min) before the next injection. For all LC–MS analyses, 5 µl of sample was injected. The column temperature was maintained at 10 °C. Creatine eluted at 7.9 min. Relative concentrations were determined from external calibration curves. Data were analysed by using MassHunter Quant (Agilent Technologies). No additional corrections were made for ion suppression; thus, concentrations are relative, not absolute.

NMR spectroscopy. Brown fat tissue samples (~20 mg) were homogenized and extracted with a mixture of ice-cold solvents water/methanol/chloroform (H_2O/MeOH/$CHCl_3$, 1:1:1 (v:v:v)). The water/methanol phase was separated and dried in a SpeedVac. The extract was reconstituted in a 550 µl mixture containing 500 µl of phosphate buffer, pH 7.4, and 50 µl of 1 mM of trimethylsilylpropanoic acid (TSP-d_4) in D_2O, vortexed for 20 s and transferred to 5-mm NMR tubes. The

NMR spectra were acquired on a Bruker 600-MHz Avance III HD spectrometer equipped with a BBI room temperature probehead and SampleJet autosampler (Bruker Biospin). ^{1}H NMR spectra were recorded by using a one-dimensional nuclear Overhauser enhancement spectroscopy pulse sequence with presaturation (noesygppr1d), collecting 256 scans with calibrated 90° pulse (~11 µs), 4.55-s acquisition time and 4-s relaxation delay. Metabolites were identified and quantified by using Chenomx NMR suite 8.2 software, by fitting the spectral lines of library compounds into the recorded NMR spectrum of tissue extract. The quantification was on the basis of peak area of TSP-d_4 signal. The metabolite concentrations are exported as micromolar values in NMR samples and normalized to wet tissue mass (nmol per mg of tissue).

Body temperature. A mouse rectal probe (World Precision Instruments) was used to examine body temperature. Mice were group-housed (three per cage) at 30 °C for 5 d. Body temperature was measured in individually housed mice at 4 °C after acclimation at 30 °C for 5 d.

Triglyceride quantification. Triglyceride content in BAT and SQ tissues was measured by using a High Sensitivity TG Assay Kit (Sigma-Aldrich, MAK264). Five standard solutions were prepared at 40, 80, 120, 160 and 200 pmol per well in 50 µl of triglyceride buffer. BAT and SQ tissues (10 mg) were weighed and homogenized in 100 µl of cold triglyceride buffer. To ensure that the lipid layer was not separated from the aqueous phase, samples were boiled for 30–45 s. Insoluble materials were removed by centrifuging the samples at 12,000*g* for 5 min. Supernatant, including the entire fat layer, was transferred into clean tubes. Each sample was then diluted 5,000× with cold triglyceride buffer and transferred to a 96-well plate at a final volume of 50 µl. Lipase (2 µl) was added to each sample, which was subsequently incubated at 37 °C for 20 min. After hydrolysis of triglycerides to glycerol and fatty acids, 50 µl of the master reaction mix was added to the wells, and the samples were incubated at 37 °C for 30 min. Fluorescence intensity was measured at $\lambda_{ex} = 535/\lambda_{em} = 587$ nm. To control for NADH and NADPH background signal, every sample was also analysed in the absence of the triglyceride enzyme mix. The reading from this control was subtracted from the sample reading.

Stromal-vascular-fraction isolation of mouse brown preadipocytes. Interscapular BAT stromal vascular fraction was obtained from 3-week-old animals (after genotyping). Interscapular BAT was dissected, washed in PBS, minced and digested for 45 min at 37 °C in isolation buffer (1.5 mg ml^{-1} collagenase B (Sigma), 123 mM NaCl, 5 mM KCl, 1.3 mM $CaCl_2$, 5 mM glucose, 100 mM HEPES and 4% BSA). The tissue suspension was filtered through a 100-µm cell strainer and centrifuged at 600*g* for 5 min to pellet the stromal vascular fraction, which was subsequently resuspended in adipocyte culture medium (DMEM/F12 (Wisent), 10% foetal bovine serum and 0.1% PenStrep), filtered through a 40-µm cell strainer, centrifuged at 600*g* for 5 min, resuspended and plated in adipocyte culture medium onto polystyrene cell culture dishes (Corning). Cells were maintained at 37 °C in 10% CO_2. Cells from five animals were plated on a single 10-cm dish, then passaged twice into ten 10-cm dishes. Cells from each 10-cm dish were frozen and stored in liquid nitrogen in freezing medium (10% DMSO, 90% foetal bovine serum) at 80% confluency.

Adipocyte differentiation. Preadipocytes were grown to post-confluency, and differentiation was induced with adipogenic cocktail (1 µM rosiglitazone, 0.5 mM isobutylmethylxanthine, 5 µM dexamethasone, 0.114 µg ml^{-1} insulin, 1 nM triiodo-L-thyronine and 125 µM indomethacin). Cells were re-fed every 48 h with maintenance cocktail (1 µM rosiglitazone and 0.5 µg ml^{-1} insulin). Cells were fully differentiated by day 6.

Adenoviral cloning, construction and transduction. *Cre* and *Gfp* were amplified with PCR, gel extracted and cloned into the pENTR Directional TOPO entry vector (Invitrogen) according to the manufacturer's instructions. Entry-vector clones were shuttled into the pAD/CMV/V5-DEST Gateway vector and digested with PacI (NEB). 293A cells were plated at 0.5×10^6 cells per well of a six-well dish and transfected 12 h later with 3 µg of PacI-linearized adenoviral plasmid. Crude adenovirus was generated according to the manufacturer's instructions (Invitrogen) and then amplified by infecting 293A cells (500 µl crude virus per 15 cm dish of 293A cells). Virus was purified by using a Fast Trap Adenovirus Purification and Concentration Kit (EMD Millipore), according to the manufacturer's instructions. Three 15-cm dishes were used for each preparation. Primary adipocytes were transduced with purified adenovirus on day 3.5 of differentiation.

Deletion of *CrT* in vitro. Preadipocytes from the BAT of *CrT*$^{lox/y}$ animals were isolated. On day 3.5 after the induction of differentiation, adipocytes were infected with GFP- or CRE-expressing adenovirus (1:500 dilution). After 12 h of infection, virus was removed, and the cells were re-fed with maintenance cocktail every 48 h thereafter. All experiments using this system were conducted from adipocytes at day 10 of differentiation, which was determined empirically to allow for sufficient time for *CrT* transcript levels to decrease significantly.

Cellular respirometry. Primary brown preadipocytes were plated at 15,000 cells per well of a XF24 V7 cell culture microplate, and differentiation was induced 12 h later. On day 10 post-differentiation, adipocytes were washed once and maintained for ~45 min in unbuffered DMEM supplemented with 1 mM pyruvate. The protocol for the XFe24 was set to analyse cellular respirometry by using a mix:wait:measure ratio of 4:2:2 min. Norepinephrine (100 nM) was used to stimulate thermogenic respiration. A mix of rotenone and antimycin A (3 µM each) was used to inhibit mitochondrial respiration.

Purification of mature mouse brown adipocytes. Interscapular BAT was digested in isolation buffer HBSS (Sigma), 2 mg ml^{-1} collagenase B (Worthington), 1 mg ml^{-1} soybean trypsin inhibitor (Worthington) and 4% BSA with continuous shaking at 37 °C for 45 min. The tissue suspension was filtered through a 100-µm cell strainer and spun at 30*g* for 5 min at room temperature. The infranatant was removed, and adipocytes were washed with 20 ml ice-cold PBS and centrifuged again. Infranatant was removed, and cells were snap-frozen in liquid nitrogen until downstream analysis.

Collection of human adipose tissue samples. Subcutaneous adipose tissue was collected under IRB 2011P000079 (approved by the Beth Israel Deaconess Medical Center Committee on Clinical Investigations) from subjects recruited from the plastic-surgeon operating-room schedule at Beth Israel Deaconess Medical Center in a consecutive fashion, as scheduling permitted, to process the sample. The inclusion criteria were healthy male and female subjects, ages 18–64 receiving abdominal surgery. The exclusion criteria were diagnosis of diabetes, any subjects taking insulin-sensitizing medications such as thiazolidinediones or metformin, chromatin-modifying enzymes such as valproic acid, and drugs known to induce insulin resistance such as mTOR inhibitors (for example, sirolimus or tacrolimus) or systemic steroid medications. Fasting serum was collected and tested for insulin, glucose, free fatty acids, and a lipid-panel was performed in a Clinical Laboratory Improvement Amendments approved laboratory. BMI measures were derived from electronic medical records and confirmed by self-reporting, and measures of insulin resistance, the homeostasis model assessment-estimated insulin resistance index (HOMA-IR) and revised quantitative insulin sensitivity check index (QUICKI) were calculated[45,46]. Female subjects in the first and fourth quartiles for either HOMA-IR or QUICKI and matched for age and BMI were processed for RNA-seq. Human participants who donated adipose tissue provided informed consent.

Purification of mature human adipocytes. Whole-tissue subcutaneous adipose specimens were freshly collected from the operating room. Skin was removed, and adipose tissue was cut into 1- to 2-inch pieces and rinsed thoroughly with 37 °C PBS to remove blood. Cleaned adipose tissue pieces were quickly minced with an electric grinder with 3/16-inch hole plate, and 400 ml of sample was placed in a 2-l wide-mouthed Erlenmeyer culture flask with 100 ml of freshly prepared blendzyme (Roche Liberase TM, research grade, cat. no. 05401127001, in PBS, at a ratio of 6.25 mg per 50 ml) and shaken in a 37 °C shaking incubator at 120 r.p.m. for 15–20 min to digest until the sample appeared uniform. Digestion was stopped with 100 ml of freshly made KRB (5.5 mM glucose, 137 mM NaCl, 15 mM HEPES, 5 mM KCl, 1.25 mM $CaCl_2$, 0.44 mM KH_2PO_4, 0.34 mM Na_2HPO_4 and 0.8 mM $MgSO_4$), supplemented with 2% BSA. Digested tissue was filtered through a 300-µM sieve and washed with KRB/albumin and flow through until only connective tissue remained. Samples were centrifuged at 233*g* for 5 min at room temperature, clear lipid was later removed, and floated adipocyte supernatant was collected, divided into aliquots and flash-frozen in liquid nitrogen.

RNA isolation from mature human adipocytes. Total RNA from ~400 µl of thawed floated adipocytes was isolated in TRIzol reagent (Invitrogen) according to the manufacturer's instructions. For RNA-seq library construction, mRNA was purified from 100 ng of total RNA by using a Ribo-Zero rRNA removal kit (Epicentre) to deplete ribosomal RNA and convert into double-stranded complementary DNA by using an NEBNext mRNA Second Strand Synthesis Module (E6111L). cDNA was subsequently tagmented and amplified for 12 cycles by using a Nextera XT DNA Library Preparation Kit (Illumina FC-131). Sequencing libraries were analysed with Qubit and Agilent Bioanalyzer, pooled at a final loading concentration of 1.8 pM and sequenced on a NextSeq500. Sequencing reads were demultiplexed by using bcl2fastq and aligned to the mm10 mouse genome by using HISAT2 (ref. [47]). PCR duplicates and low-quality reads were removed by Picard (https://broadinstitute.github.io/picard). Filtered reads were assigned to the annotated transcriptome and quantified by using featureCounts[48].

Gene expression analysis (RT–qPCR). Total RNA was extracted from frozen tissue by using TRIzol (Invitrogen), purified with RNeasy Mini spin columns (QIAGEN) and reverse transcribed by using a High-Capacity cDNA Reverse Transcription kit (Applied Biosystems). The resultant cDNA was analysed by RT–qPCR. Briefly, 20 ng cDNA and 150 nmol of each primer were mixed with GoTaq qPCR Master Mix (Promega). Reactions were performed in a 384-well format by using a CFX384 Real-time PCR system (Bio-Rad). Normalized mRNA expression was calculated by using the ΔΔCt method, using *Ppib* mRNA as the reference gene. The list of primer sequences can be found in Supplementary Table 1.

BAT lysis, protein digestion and peptide tandem mass tag (TMT) labelling. BAT was mechanically lysed in ice-cold lysis buffer (50 mM Tris pH 8.5, 50 mM β-glycerophosphate, 1 mM sodium orthovanadate, 1 mM PMSF and EDTA-free protease-inhibitor cocktail in 2% SDS). The lysate was centrifuged at 10,000*g* for 10 min. Protein content was measured with using a BCA assay (Thermo Scientific); disulfide bonds were reduced with 5 mM tris(2-carboxyethyl)phosphine, and cysteine residues were alkylated with iodoacetamide (14 mM). Protein lysates were purified by methanol–chloroform precipitation and digested overnight with LysC (Wako) in a 1/200 enzyme/protein ratio in 2 M urea and 25 mM Tris-HCl, pH 8.5. The digest was acidified with 10% formic acid to a pH of ~2–3 and subjected to C18 solid-phase extraction (50 mg cartridges) (Sep-Pak, Waters). Isobaric labelling of the digested peptides was accomplished with 10-plex TMT reagents (ThermoFisher Scientific). Reagents, 5 mg, were dissolved in 252 µl ACN, and one-quarter of the solution was added to 100 µg of peptides dissolved in 100 µl of 200 mM HEPES, pH 8.5. After 1 h (room temperature), the reaction was quenched by addition of 3 µl of 5% hydroxylamine. Labelled peptides were combined and acidified before C18 solid-phase extraction on Sep-Pak cartridges (50 mg).

Basic pH reversed-phase separation. TMT-labelled peptides were solubilized in 500 µl solution containing 5% ACN/10 mM ammonium bicarbonate, pH 8.0 and separated by an Agilent 300 Extend C18 column (5-µm particles, 2.6-mm internal diameter and 220 mm in length). An Agilent 1100 binary pump coupled with a photodiode array detector (ThermoScientific) was used to separate the peptides. A 45-min linear gradient from 18–45% acetonitrile in 10 mM ammonium bicarbonate pH 8.0 (flow rate of 0.8 ml min^{-1}) separated the peptide mixtures into a total of 96 fractions (36 s). A total of 96 fractions were consolidated into 24 samples in a chequerboard fashion, acidified with 20 µl of 20% formic acid and vacuum dried to completion. Each sample was re-dissolved in 12 µl 5% formic acid/ 5% ACN, and desalted before LC–MS/MS analysis.

LC–MS/MS. Data were collected by using an Orbitrap Fusion Lumos mass spectrometer (ThermoFisher Scientific) coupled with a Proxeon EASY-nLC 1200 LC pump (ThermoFisher Scientific). Peptides were separated on a microcapillary column (75-µm inner diameter) packed with 35 cm of Accucore C18 resin (2.6 µm, 100 Å; ThermoFisher Scientific). Peptides were separated by using a 3-h gradient of 6–27% acetonitrile in 0.125% formic acid with a flow rate of 400 nl min^{-1}. The data were acquired by using a mass range of *m/z* 350–1,350, resolution 120,000, automatic gain control target 1×10^6, maximum injection time 100 ms, dynamic exclusion of 120 s for the peptide measurements in the Orbitrap. Data-dependent MS/MS spectra were acquired in the ion trap with a normalized collision energy set at 35%, automatic gain control target set to 1.8×10^4 and a maximum injection time of 120 ms. Three-stage mass spectrometry scans were acquired in the Orbitrap with a higher-energy collisional dissociation energy set to 55%, the automatic gain control target set to 1.5×10^5, a maximum injection time of 150 ms, resolution at 15,000 and a maximum synchronous precursor selection set to 10.

Data processing and spectra assignment. A compendium of in-house-developed software was used to convert mass spectrometric data (Raw file) to the mzXML format, as well as to correct monoisotopic *m/z* measurements and erroneous assignments of peptide charge state[49]. All experiments used the Mouse UniProt database (downloaded 10 April 2017) wherein reversed protein sequences and known contaminants such as human keratins were appended. SEQUEST searches were performed by using a 20-p.p.m. precursor-ion tolerance, while requiring each peptide's amino/carboxy (N/C) terminus to have trypsin protease specificity and allowing up to two missed cleavages. 10-plex TMT tags on peptide N termini and lysine residues (+229.162932 Da) and carbamidomethylation of cysteine residues (+57.02146 Da) were set as static modifications, while methionine oxidation (+15.99492 Da) was set as variable modification. A MS/MS spectra assignment FDR of less than 1% was achieved by applying the target–decoy database search strategy[49]. Filtering was performed by using an in-house linear discrimination analysis method to create one combined filter parameter from the following peptide-ion and MS/MS spectra metrics: SEQUEST parameters XCorr and ΔCn, peptide-ion mass accuracy and charge state, in-solution charge of peptide, peptide length and mis-cleavages. Linear discrimination scores were used to assign probabilities to each MS/MS spectrum for being assigned correctly and these probabilities were further used to filter the dataset with a MS/MS spectra assignment FDR of smaller than a 1% at the protein level[50].

Determination of TMT reporter-ion intensities and quantitative data analysis. For quantification, a 0.03 *m/z* window centred on the theoretical *m/z* value of each the ten reporter ions and the intensity of the signal closest to the theoretical *m/z* value was recorded. Reporter-ion intensities were further de-normalized on the basis of their ion accumulation time for each MS/MS or or three-stage MS spectrum and adjusted on the basis of the overlap of isotopic envelopes of all reporter ions (as determined by the manufacturer). The total signal intensity across all peptides quantified was summed for each TMT channel, and all intensity values were adjusted to account for potentially uneven TMT labelling and/or sample handling variance.

Proteomic data processing and quality control. Two proteomic assays were performed to determine expression changes between $CrT^{tox/y}$ and AdCrTKO animals at 30 °C ($n = 10$) and 22 °C ($n = 10$) conditions. Expression measurements were successfully obtained across all samples in both assays for 5,508 unique proteins. We did not consider proteins that could not be measured in all conditions. Expression values were $\log_2$-transformed, and their distribution was visualized as a mean of quality control. We then performed a principal component analysis of expression values for the 50 proteins showing the highest variance across samples, by using the prcomp() function in R (v3.4.2.). It is important to note that, because 30 °C and 22 °C BAT were processed independently in our proteomics workflow, most differences were probably due to batch effects and not to temperature. Regardless, while the samples segregated by assay on the first principal component, a clear difference was observed between the $CrT^{tox/y}$ and AdCrTKO genotypes on the second principal component. Similar results were obtained when using 100 or 200 highest variance peptides. The principal component analysis plot was produced in R using ggplot2 (v3.0.0) and ggfortify (v0.4.5.) package.

Differential protein expression. We determined proteins exhibiting differential expression between $CrT^{tox/y}$ and AdCrTKO BAT at 30 °C ($n = 10$) and 22 °C ($n = 10$) by performing moderated *t*-tests using the limma (v3.32.10) package in R[51,52], as justified in ref. [53]. *P* values were adjusted for multiple testing by using the Benjamini–Hochberg approach. In R code, this translates to:

fit <- eBayes(lmFit(expression, model.matrix(~temperature + genotype)))
results = topTable(fit, coef = "genotypeKO", number = Inf, adjust.method = "BH", lfc = 0).

This led to 15 proteins differentially expressed at 0.05 FDR. The volcano plot was produced with the ggplot2 (v3.0.0) package in R.

Gene ontology enrichment. To find gene ontology terms enriched in the set of differentially expressed peptides (15) with respect to the complete set of tested peptides (5,508), we used the GOrilla tool[54] with the 'two unranked lists of genes' option and a *P*-value threshold of 1×10^{-3} (*Mus musculus* organism, database update 18 August 2018).

Statistical analyses. Results are presented as mean ± s.e.m. Unpaired two-tailed Student's *t*-test for pairwise comparison, one-way ANOVA for multiple comparisons, *F*-test for linear regression and ANCOVA for in vivo metabolic analyses were used to calculate *P* values to determine statistical differences. Significance was considered as $P < 0.05$. Statistical analysis and plotting for metabolic studies were performed in the R programming language with CalR, a custom package for analysis of indirect calorimetry using analysis of covariance with a graphical user interface. Mice were randomly assigned to treatment groups for in vivo studies. Values for *n* represent biological replicates for cultured cell experiments or individual animals for in vivo experiments. Specific details for *n* values are noted in each figure legend.

Reporting Summary. Further information on research design is available in the Nature Research Reporting Summary linked to this article.

Data availability

All proteomic data generated or analysed during this study are included in this published article (and its supplementary information files). Additional data that support the findings of this study are available from the corresponding authors on reasonable request.

Received: 13 July 2018; Accepted: 15 January 2019;
Published online: 25 February 2019

References

1. Lengyel, E., Makowski, L., DiGiovanni, J. & Kolonin, M. G. Cancer as a matter of fat: the crosstalk between adipose tissue and tumors. *Trends Cancer* **4**, 374–384 (2018).
2. Twig, G. et al. Body-mass index in 2.3 million adolescents and cardiovascular death in adulthood. *N. Engl. J. Med.* **374**, 2430–2440 (2016).
3. Ravussin, E. et al. Reduced rate of energy expenditure as a risk factor for body-weight gain. *N. Engl. J. Med.* **318**, 467–472 (1988).
4. Jung, R. T., Shetty, P. S., James, W. P., Barrand, M. A. & Callingham, B. A. Reduced thermogenesis in obesity. *Nature* **279**, 322–323 (1979).
5. Hofmann, W. E., Liu, X., Bearden, C. M., Harper, M. E. & Kozak, L. P. Effects of genetic background on thermoregulation and fatty acid-induced uncoupling of mitochondria in UCP1-deficient mice. *J. Biol. Chem.* **276**, 12460–12465 (2001).
6. Liu, X. et al. Paradoxical resistance to diet-induced obesity in UCP1-deficient mice. *J. Clin. Invest.* **111**, 399–407 (2003).
7. Mottillo, E. P. et al. Coupling of lipolysis and de novo lipogenesis in brown, beige, and white adipose tissues during chronic beta3-adrenergic receptor activation. *J. Lipid Res.* **55**, 2276–2286 (2014).

8. Muller, S. et al. Proteomic analysis of human brown adipose tissue reveals utilization of coupled and uncoupled energy expenditure pathways. *Sci. Rep.* **6**, 30030 (2016).
9. Rowland, L. A., Maurya, S. K., Bal, N. C., Kozak, L. & Periasamy, M. Sarcolipin and uncoupling protein 1 play distinct roles in diet-induced thermogenesis and do not compensate for one another. *Obesity (Silver Spring)* **24**, 1430–1433 (2016).
10. Ukropec, J., Anunciado, R. P., Ravussin, Y., Hulver, M. W. & Kozak, L. P. UCP1-independent thermogenesis in white adipose tissue of cold-acclimated Ucp1$^{-/-}$ mice. *J. Biol. Chem.* **281**, 31894–31908 (2006).
11. Ikeda, K. et al. UCP1-independent signaling involving SERCA2b-mediated calcium cycling regulates beige fat thermogenesis and systemic glucose homeostasis. *Nat. Med.* **23**, 1454–1465 (2017).
12. Bertholet, A. M. et al. Mitochondrial patch clamp of beige adipocytes reveals UCP1-positive and UCP1-negative cells both exhibiting futile creatine cycling. *Cell Metab.* **25**, 811–822 e814 (2017).
13. Kazak, L. et al. A creatine-driven substrate cycle enhances energy expenditure and thermogenesis in beige fat. *Cell* **163**, 643–655 (2015).
14. Wakatsuki, T. et al. Thermogenic responses to high-energy phosphate contents and/or hindlimb suspension in rats. *Jpn J. Physiol.* **46**, 171–175 (1996).
15. Yamashita, H. et al. Increased growth of brown adipose tissue but its reduced thermogenic activity in creatine-depleted rats fed beta-guanidinopropionic acid. *Biochim. Biophys. Acta* **1230**, 69–73 (1995).
16. Kazak, L. et al. Genetic depletion of adipocyte creatine metabolism inhibits diet-induced thermogenesis and drives obesity. *Cell Metab.* **26**, 660–671 e663 (2017).
17. Fitch, C. D., Shields, R. P., Payne, W. F. & Dacus, J. M. Creatine metabolism in skeletal muscle. 3. Specificity of the creatine entry process. *J. Biol. Chem.* **243**, 2024–2027 (1968).
18. Berlet, H. H., Bonsmann, I. & Birringer, H. Occurrence of free creatine, phosphocreatine and creatine phosphokinase in adipose tissue. *Biochim. Biophys. Acta* **437**, 166–174 (1976).
19. Skelton, M. R. et al. Creatine transporter (CrT; Slc6a8) knockout mice as a model of human CrT deficiency. *PLoS ONE* **6**, e16187 (2011).
20. Lee, J., Choi, J., Aja, S., Scafidi, S. & Wolfgang, M. J. Loss of adipose fatty acid oxidation does not potentiate obesity at thermoneutrality. *Cell Rep.* **14**, 1308–1316 (2016).
21. Kazak, L. et al. UCP1 deficiency causes brown fat respiratory chain depletion and sensitizes mitochondria to calcium overload-induced dysfunction. *Proc. Natl Acad. Sci. USA* **114**, 7981–7986 (2017).
22. Eguchi, J. et al. Transcriptional control of adipose lipid handling by IRF4. *Cell Metab.* **13**, 249–259 (2011).
23. Speakman, J. R., Krol, E. & Johnson, M. S. The functional significance of individual variation in basal metabolic rate. *Physiol. Biochem. Zool.* **77**, 900–915 (2004).
24. Bloom, J. D. et al. Disodium (R,R)-5-[2-[[2-(3-chlorophenyl)-2-hydroxyethyl]-amino] propyl]-1,3-benzodioxole-2,2-dicarboxylate (CL 316,243). A potent beta-adrenergic agonist virtually specific for beta 3 receptors. A promising antidiabetic and antiobesity agent. *J. Med. Chem.* **35**, 3081–3084 (1992).
25. Himms-Hagen, J., Hogan, S. & Zaror-Behrens, G. Increased brown adipose tissue thermogenesis in obese (ob/ob) mice fed a palatable diet. *Am. J. Physiol.* **250**, E274–E281 (1986).
26. Bachman, E. S. et al. betaAR signaling required for diet-induced thermogenesis and obesity resistance. *Science* **297**, 843–845 (2002).
27. Rothwell, N. J. & Stock, M. J. A role for brown adipose tissue in diet-induced thermogenesis. *Nature* **281**, 31–35 (1979).
28. Leibel, R. L. & Hirsch, J. Diminished energy requirements in reduced-obese patients. *Metabolism* **33**, 164–170 (1984).
29. Eringa, E. C. et al. Regulation of vascular function and insulin sensitivity by adipose tissue: focus on perivascular adipose tissue. *Microcirculation* **14**, 389–402 (2007).
30. Singhal, A. et al. Influence of leptin on arterial distensibility: a novel link between obesity and cardiovascular disease? *Circulation* **106**, 1919–1924 (2002).
31. Shimizu, I. et al. Vascular rarefaction mediates whitening of brown fat in obesity. *J. Clin. Invest.* **124**, 2099–2112 (2014).
32. Ernande, L. et al. Relationship of brown adipose tissue perfusion and function: a study through beta2-adrenoreceptor stimulation. *J. Appl. Physiol. (1985)* **120**, 825–832 (2016).
33. Hankir, M. K. & Klingenspor, M. Brown adipocyte glucose metabolism: a heated subject. *EMBO Rep.* **19**, e46404 (2018).
34. Cereijo, R. et al. CXCL14, a brown adipokine that mediates brown-fat-to-macrophage communication in thermogenic adaptation. *Cell Metab.* **28**, 750–763.e6 (2018).
35. Rosell, M. et al. Brown and white adipose tissues: intrinsic differences in gene expression and response to cold exposure in mice. *Am. J. Physiol. Endocrinol. Metab.* **306**, E945–E964 (2014).
36. Svensson, P. A. et al. Gene expression in human brown adipose tissue. *Int. J. Mol. Med.* **27**, 227–232 (2011).
37. Gerngross, C., Schretter, J., Klingenspor, M., Schwaiger, M. & Fromme, T. Active brown fat during (18)F-FDG PET/CT imaging defines a patient group with characteristic traits and an increased probability of brown fat redetection. *J. Nucl. Med.* **58**, 1104–1110 (2017).
38. Din, M. U. et al. Postprandial oxidative metabolism of human brown fat indicates thermogenesis. *Cell Metab.* **28**, 207–216.e3 (2018).
39. Fischer, A. W., Cannon, B. & Nedergaard, J. Optimal housing temperatures for mice to mimic the thermal environment of humans: an experimental study. *Mol. Metab.* **7**, 161–170 (2018).
40. Speakman, J. R. & Keijer, J. Not so hot: Optimal housing temperatures for mice to mimic the thermal environment of humans. *Mol. Metab.* **2**, 5–9 (2012).
41. Wada, S. et al. The tumor suppressor FLCN mediates an alternate mTOR pathway to regulate browning of adipose tissue. *Genes Dev.* **30**, 2551–2564 (2016).
42. Perna, M. K. et al. Creatine transporter deficiency leads to increased whole body and cellular metabolism. *Amino Acids* **48**, 2057–2065 (2016).
43. Streijger, F. et al. Mice lacking brain-type creatine kinase activity show defective thermoregulation. *Physiol. Behav.* **97**, 76–86 (2009).
44. Fuhrer, T., Heer, D., Begemann, B. & Zamboni, N. High-throughput, accurate mass metabolome profiling of cellular extracts by flow injection-time-of-flight mass spectrometry. *Anal. Chem.* **83**, 7074–7080 (2011).
45. Katz, A. et al. Quantitative insulin sensitivity check index: a simple, accurate method for assessing insulin sensitivity in humans. *J. Clin. Endocrinol. Metab.* **85**, 2402–2410 (2000).
46. Matthews, D. R. et al. Homeostasis model assessment: insulin resistance and beta-cell function from fasting plasma glucose and insulin concentrations in man. *Diabetologia* **28**, 412–419 (1985).
47. Kim, D., Langmead, B. & Salzberg, S. L. HISAT: a fast spliced aligner with low memory requirements. *Nat. Methods* **12**, 357–360 (2015).
48. Liao, Y., Smyth, G. K. & Shi, W. featureCounts: an efficient general purpose program for assigning sequence reads to genomic features. *Bioinformatics* **30**, 923–930 (2014).
49. Elias, J. E. & Gygi, S. P. Target-decoy search strategy for increased confidence in large-scale protein identifications by mass spectrometry. *Nat. Methods* **4**, 207–214 (2007).
50. Huttlin, E. L. et al. A tissue-specific atlas of mouse protein phosphorylation and expression. *Cell* **143**, 1174–1189 (2010).
51. Ritchie, M. E. et al. limma powers differential expression analyses for RNA-sequencing and microarray studies. *Nucleic Acids Res.* **43**, e47 (2015).
52. Smyth, G. K. Linear models and empirical bayes methods for assessing differential expression in microarray experiments. *Stat. Appl. Genet. Mol. Biol.* **3**, Article3 (2004).
53. Kammers, K., Cole, R. N., Tiengwe, C. & Ruczinski, I. Detecting significant changes in protein abundance. *EuPA Open Proteom.* **7**, 11–19 (2015).
54. Eden, E., Navon, R., Steinfeld, I., Lipson, D. & Yakhini, Z. GOrilla: a tool for discovery and visualization of enriched GO terms in ranked gene lists. *BMC Bioinformatics* **10**, 48 (2009).

Acknowledgements

This work was supported by the Canadian Institutes of Health Research (CIHR; grant PJT-159529), Goodman Cancer Research Centre and McGill University New Investigator Program, and DK114528-01 NIH/NIDDK K99 Pathway to Independence award (to L.K.). We acknowledge funding from a Canderel Fellowship (to J.F.R.). We acknowledge technical assistance from the McGill/GCRC Metabolomics core facility. The GCRC Metabolomics Core Facility is funded by the Dr. John R and Clara M. Fraser Memorial Trust, the Terry Fox Foundation, the Québec Breast Cancer Foundation and McGill University. We acknowledge funding from NIH R01HL 85744 and U24DK100469 Mayo Clinic Metabolomics Resource Core (to P.D.), AHA 13POST14540015 and NIH/NIDDK P30 DK057521 (to L.T.), NIH/NIDDK P30 DK057521, NIH/NIDDK R01 DK102173 and R01 ES017690 (to E.D.R.), and NIH DK31405 and JPB Foundation (to B.M.S.).

Author contributions

L.K. conceptualized the study, designed research, performed biochemical, cellular and in vivo experiments, analysed data and wrote the paper. J.F.R., B.S., G.Z.L. and F.Y.D. performed in vivo experiments. M.P.J. performed proteomics experiments. M.L., L.C.R. and I.R.W. analysed proteomics data. S.Z. performed and analysed NMR experiments. E.T.C., P.D. and E.D.R. provided resources. L.T. recruited human subjects and isolated adipocytes, and D.T. performed RNA-seq experiments. L.K. and B.M.S. co-wrote the paper, with assistance from co-authors.

Competing interests

The authors declare no competing interests.

Additional information

Supplementary information is available for this paper at https://doi.org/10.1038/s42255-019-0035-x.

Reprints and permissions information is available at www.nature.com/reprints.

Correspondence and requests for materials should be addressed to L.K. or B.M.S.

Publisher's note: Springer Nature remains neutral with regard to jurisdictional claims in published maps and institutional affiliations.

nature research

Corresponding author(s): Lawrence Kazak, Bruce M. Spiegelman

Last updated by author(s): Jan 4, 2019

Reporting Summary

Nature Research wishes to improve the reproducibility of the work that we publish. This form provides structure for consistency and transparency in reporting. For further information on Nature Research policies, see Authors & Referees and the Editorial Policy Checklist.

Statistics

For all statistical analyses, confirm that the following items are present in the figure legend, table legend, main text, or Methods section.

n/a	Confirmed
☐	☒ The exact sample size (*n*) for each experimental group/condition, given as a discrete number and unit of measurement
☐	☒ A statement on whether measurements were taken from distinct samples or whether the same sample was measured repeatedly
☐	☒ The statistical test(s) used AND whether they are one- or two-sided *Only common tests should be described solely by name; describe more complex techniques in the Methods section.*
☒	☐ A description of all covariates tested
☐	☒ A description of any assumptions or corrections, such as tests of normality and adjustment for multiple comparisons
☐	☒ A full description of the statistical parameters including central tendency (e.g. means) or other basic estimates (e.g. regression coefficient) AND variation (e.g. standard deviation) or associated estimates of uncertainty (e.g. confidence intervals)
☐	☒ For null hypothesis testing, the test statistic (e.g. *F*, *t*, *r*) with confidence intervals, effect sizes, degrees of freedom and *P* value noted *Give P values as exact values whenever suitable.*
☒	☐ For Bayesian analysis, information on the choice of priors and Markov chain Monte Carlo settings
☒	☐ For hierarchical and complex designs, identification of the appropriate level for tests and full reporting of outcomes
☒	☐ Estimates of effect sizes (e.g. Cohen's *d*, Pearson's *r*), indicating how they were calculated

Our web collection on statistics for biologists contains articles on many of the points above.

Software and code

Policy information about availability of computer code

Data collection	NMR: Chenomx NMR suite 8.2 QPCR: CFX Maestro 2017 Seahorse: Wave 2.4
Data analysis	Peptide mass spectra were processed with an house SEQUEST-based software pipeline (Huttlin, E.L., et all. Cell. 143, 1174–1189 (2010). Details available upon reasonable request GraphPad Prism, 7 Microsoft office Excel 2016 limma (v3.32.10) package in R

For manuscripts utilizing custom algorithms or software that are central to the research but not yet described in published literature, software must be made available to editors/reviewers. We strongly encourage code deposition in a community repository (e.g. GitHub). See the Nature Research guidelines for submitting code & software for further information.

Data

Policy information about availability of data

All manuscripts must include a data availability statement. This statement should provide the following information, where applicable:

- Accession codes, unique identifiers, or web links for publicly available datasets
- A list of figures that have associated raw data
- A description of any restrictions on data availability

The data that support the findings of this study are available from the corresponding author upon request.

Field-specific reporting

Please select the one below that is the best fit for your research. If you are not sure, read the appropriate sections before making your selection.

☒ Life sciences ☐ Behavioural & social sciences ☐ Ecological, evolutionary & environmental sciences

For a reference copy of the document with all sections, see nature.com/documents/nr-reporting-summary-flat.pdf

Life sciences study design

All studies must disclose on these points even when the disclosure is negative.

Sample size	Sample sizes were predetermined based on effect size, standard deviation, and significance level required to attain statistical significance of p<0.05 with a 90% probability on the basis of previous experiments using similar methodologies and were deemed sufficient to account for any biological/technical variability.
Data exclusions	No data were excluded
Replication	All attempts of in vivo replication were successful. Proteomics was performed with five independent samples at two environmental temperatures. Only replicated proteomic data are discussed, effectively increasing independent sample number to 10 per genotype. Proteomic data were further followed up by alternative approaches, such as RT-qPCR.
Randomization	For in vivo studies, mice in each genotype were randomly assigned to treatment groups. For MS analyses, samples were processed in random order and experimenters were blinded to experimental conditions.
Blinding	For MS analyses, samples were processed in random order and experimenters were blinded to experimental conditions.

Reporting for specific materials, systems and methods

We require information from authors about some types of materials, experimental systems and methods used in many studies. Here, indicate whether each material, system or method listed is relevant to your study. If you are not sure if a list item applies to your research, read the appropriate section before selecting a response.

Materials & experimental systems

n/a	Involved in the study
☒	☐ Antibodies
☐	☒ Eukaryotic cell lines
☒	☐ Palaeontology
☐	☒ Animals and other organisms
☐	☒ Human research participants
☒	☐ Clinical data

Methods

n/a	Involved in the study
☒	☐ ChIP-seq
☒	☐ Flow cytometry
☒	☐ MRI-based neuroimaging

Eukaryotic cell lines

Policy information about cell lines

Cell line source(s)	Primary brown adipocytes from CrT(lox/y) mice (strain: C57BL6/J, Stock#: 000664). Mice were bred and cells were isolated in-house.
Authentication	N/A
Mycoplasma contamination	N/A
Commonly misidentified lines (See ICLAC register)	No commonly misidentified cell lines were used

Animals and other organisms

Policy information about studies involving animals; ARRIVE guidelines recommended for reporting animal research

Laboratory animals	Mice were housed at 22°C under a 12 hr light/dark cycle with free access to food and water until 8 weeks of age. CrT(lox/y) animals were obtained from the Jackson Laboratory [B6(SJL)-Slc6a8tm1.1Clar/J), Stock No: 020642]. Adiponectin-Cre mice (B6;FVB-Tg(Adipoq-cre)1Evdr/J, Stock No: 010803), maintained on a C57BL/6J background, were bred to CrT(lox/y) animals to generate experimental groups. All experiments used age-matched male littermates and were conducted at either 30°C or 22°C. Animal experiments were performed according to procedures approved by the Animal Resource Centre at McGill University and

	comply with guidelines set by the Canadian Council of Animal Care, and experiments were performed according to procedures approved by the Institutional Animal Care and Use Committee (IACUC) of the Beth Israel Deaconess Medical Center or the Harvard Center for Comparative Medicine. Unless otherwise stated, mice used were age-matched littermates (8–12 weeks of age), and housed in at (22 °C or 30 °C) on a 12 h light/dark cycle. AdCrTKO (CrT[lox/y]; AdipoQ-Cre) and age-matched littermates (CrT[lox/y]) were used. Brown adipocytes were cultured from male and female pups after genotyping (14 days old).
Wild animals	N/A
Field-collected samples	N/A
Ethics oversight	Animal experiments were performed according to procedures approved by the Animal Resource Centre at McGill University and comply with guidelines set by the Canadian Council of Animal Care. Experiments were performed according to procedures approved by the Institutional Animal Care and Use Committee (IACUC) of the Beth Israel Deaconess Medical Center.

Note that full information on the approval of the study protocol must also be provided in the manuscript.

Human research participants

Policy information about studies involving human research participants

Population characteristics	Inclusion criteria included healthy male and female subjects, ages 18-64 receiving abdominal surgery. Exclusion criteria were diagnosis of diabetes, any subjects taking insulin-sensitizing medications like thiazolidinediones or metformin, chromatin modifying enzymes such as valproic acid, and drugs known to induce insulin resistance such as mTOR inhibitors (e.g. sirolimus, tacrolimus) or systemic steroid medications.
Recruitment	Subjects recruited from plastic surgeon operating room schedule at Beth Israel Deaconess Medical Center in consecutive fashion as scheduling permitted to process the sample.
Ethics oversight	Subcutaneous adipose tissue was collected under IRB 2011P000079, and approved by the Beth Israel Deaconess Medical Center Committee on Clinical Investigations

Note that full information on the approval of the study protocol must also be provided in the manuscript.